Nano Energy 69 (2020) 104474

Contents lists available at ScienceDirect

Nano Energy

journal homepage: http://www.elsevier.com/locate/nanoen

Full paper

Both cationic and anionic redox chemistry in a P2-type sodium layered oxide

Peng-Fei Wang [a,1], Yao Xiao [b,1], Nan Piao [a,1], Qin-Chao Wang [c], Xiao Ji [a], Ting Jin [a], Yu-Jie Guo [b], Sufu Liu [a], Tao Deng [a], Chunyu Cui [a], Long Chen [a], Yu-Guo Guo [b], Xiao-Qing Yang [c], Chunsheng Wang [a,*]

[a] Department of Chemical and Biomolecular Engineering, University of Maryland, College Park, MD, 20742, USA
[b] CAS Key Laboratory of Molecular Nanostructure and Nanotechnology, CAS Research/Education Center for Excellence in Molecular Sciences, Beijing National Laboratory for Molecular Sciences (BNLMS), Institute of Chemistry, Chinese Academy of Sciences (CAS), Beijing, 100190, PR China
[c] Brookhaven National Laboratory, Upton, NY, 11973, USA

ARTICLE INFO

Keywords:
Sodium-ion batteries
Cathode
Anionic redox
P2-type
Electrochemistry

ABSTRACT

The demand for high energy Na-ion batteries has promoted intensive research on high energy oxygen redox chemistry in layered transition metal oxide cathodes. However, most layered cathodes with oxygen redox might suffer from irreversible electrochemical reaction, fast capacity decay and underlying O_2 release. Herein, we report that copper element with a strong electronegativaty can stablize Na-deficient P2-$Na_{2/3}Mn_{0.72}Cu_{0.22}Mg_{0.06}O_2$ phase to achieve both cationic and anionic redox chemistry. Hard and soft X-ray absorption spectra demonstrate that all Mn^{3+}/Mn^{4+}, Cu^{2+}/Cu^{3+} and $O^{2-}/(O_2)^{n-}$ participate in the redox reaction upon Na^+ ions extraction and insertion. Density functional theory (DFT) calculations confirm that the strong covalency between copper and oxygen ensures the cationic and anionic redox activity in P2-$Na_{2/3}Mn_{0.72}Cu_{0.22}Mg_{0.06}O_2$ phase. The P2-$Na_{2/3}Mn_{0.72}Cu_{0.22}Mg_{0.06}O_2$ cathode could deliver stable cycling life with 87.9% capacity retention at 1C during 100 cycles, as well as high rate performance (70.3 mA h g^{-1} cycled at 10C). Our findings not only provide a promising guidelines to enhance the electrochemical performance of layered oxides based on anionic redox activity, but also explore the potential science behind oxygen redox process.

1. Introduction

Na-ion batteries (NIBs) are known as potential alternatives to the current Li-ion battery technology for large-scale energy storage applications owing to the low cost and abundant sodium resources [1–4]. Considerable reports have been focused on the family of Na-based layered oxide cathode with different transition metal compositions, denoted as Na_xMO_2 (M = transition metal) [5–7]. Inspired by Li-rich layered manganese based oxides, denoted as $xLi_2MnO_3{\cdot}(1\text{-}x){\cdot}LiMO_2$ [8–11], which can offer high specific capacities of >200 mA h g^{-1} from cationic (transition metal valence variation) and anionic (oxygen valence variation) redox processes, the discovery of oxygen-related anionic redox activity in Na-based layered oxides might open up a feasible solution to elevate cathode capacity.

Several Na-rich or Na-deficient materials, such as Na_2IrO_3 [12] and $Na_{0.78}Ni_{0.23}Mn_{0.69}O_2$ [13], exhibit anionic redox originating from the emergence of nonbonding O (2p) orbitals. In Na-rich materials, Na ions occupy both Na layers and M layers [14,15], as a result, Na^+–O–Na^+ interactions tend to form due to the overlap between O 2p orbitals and Na 3s orbitals in the neighboring Na and M layers. It is well acknowledged that the relatively ionic nature of Na^+–O–Na^+ interactions is responsible for the oxygen redox [14,16–18]. Unfortunately, the oxygen may release from the lattice in these Na-rich compounds. On the other hand, substituting part of Li, Mg and Zn within the transition metal slabs in Na-deficient P2-$Na_{2/3}MnO_2$ materials can also create O (2p) nonbonding orbitals over O valence bond [19–21]. However, many reported oxygen-participated Na-deficient materials face challenges of the irreversible electrochemical reaction upon charging/discharging. Since the observed Na–O, Li–O, Mg–O, and Zn–O bond are all ionic, it is indispensable to explore the effect of bond ionicity/covalency on the

* Corresponding author.
E-mail address: cswang@umd.edu (C. Wang).
[1] These authors contributed equally to this work.

https://doi.org/10.1016/j.nanoen.2020.104474
Received 28 November 2019; Received in revised form 6 January 2020; Accepted 7 January 2020
Available online 10 January 2020
2211-2855/Published by Elsevier Ltd.

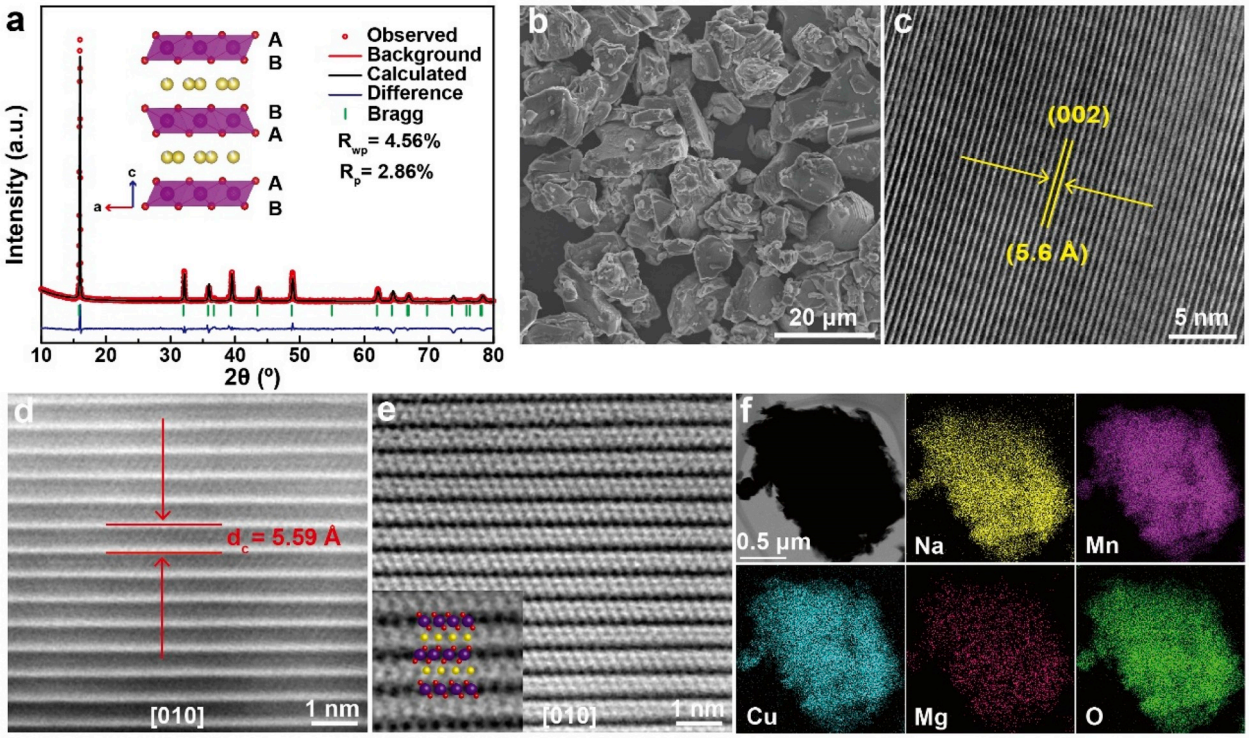

Fig. 1. (a) Powder XRD pattern and Rietveld refinement plot of the as-prepared P2-NaMCM sample. (b) SEM image (d) HR-TEM image of P2-NaMCM samples. (d) HAADF-STEM and (e) ABF-STEM images of P2-NaMCM samples at the [010] zone axis. (f) EDS maps of P2-NaMCM samples, demonstrating an even distribution of sodium, manganese, copper, magnesium and oxygen elements in sample particles.

reversibility of cationic/anionic redox.

In this work, considering the large Pauling electronegativity difference of Cu (1.90) with Na (0.93), Li (0.98), Mg (1.33), Zn (1.65), incorporating a more electronegative Cu element might make Cu–O bonds more covalent so that electrons are inclined to delocalize on the copper cations and oxygen anions. P2-$Na_{2/3}Mn_{0.72}Cu_{0.22}Mg_{0.06}O_2$ phase is thus synthesized to investigate the anionic and cationic redox activity in Na-ion cells. P2-$Na_{2/3}Mn_{0.72}Cu_{0.22}Mg_{0.06}O_2$ phase delivers a reversible capacity of 107.6 mA h g^{-1}, stable cycling performance (≈87.9% capacity retention at 1C after 100 cycles), high rate capability (70.3 mA h g^{-1} cycled at 10C) based on Mn^{3+}/Mn^{4+}, Cu^{2+}/Cu^{3+} and $O^{2-}/(O_2)^{n-}$ active redox center as evidenced by *ex situ* hard and soft X-ray absorption spectroscopy (XAS) characterization. The density functional theory (DFT) calculations confirm that such cationic and anionic redox chemistry is associated with the covalency of Cu–O bond.

2. Experimental section

2.1. Materials preparation

The P2-$Na_{2/3}Mn_{0.72}Cu_{0.22}Mg_{0.06}O_2$ sample were prepared by a solid state reaction method. The mixing of stoichiometric values of Na_2CO_3 (5mol % excess), Mn_2O_3 CuO and MgO were well ground using a mortar and pressed into pellets, followed by calcination at 1000 °C under air for 15 h and stored in an argon-filled glove box until use.

2.2. Materials characterization

The powder XRD patterns were measured by using a Bruker D8 diffractometer equipped with Cu Kα radiation (λ = 1.5418 Å). A TOPAS software was used to conduct Rietveld refinement to obtain crystal structure parameters. The morphologies of the materials were examined using a Hitachi SU-70 field-emission scanning electron microscope and transmission electron microscope (JEOL 2100) with an accelerating voltage of 200 kV. The HAADF and ABF imaging at atomic resolution was observed by a JEOL ARM200F (JEOL, Tokyo, Japan) STEM equipped with double hexapole Cs correctors (CEOS GmbH, Heidelberg, Germany) and cold filed-emission gun at 200 kV. XAS tests were conducted in transmission mode at the beamlines 7-BM of the National Synchrotron Light Source II at Brookhaven National Laboratory. The electrode samples with different charged and discharged states were sealed in water- and air-resistant polymer film in the Ar-filled glove box.

2.3. Electrochemical characterization

The working electrode was prepared by the slurry of 70 wt% active material, 20 wt% carbon black, and 10 wt% poly (vinyl difluoride) (PVDF, Aldrich) binder then the slurry were coated onto aluminum foil. A Coin-type (CR2032) cells were assembled using Na foil as the anode, the working electrode as the cathode, porous glass fiber (GF/D) as the separator, and 1 M $NaClO_4$ dissolved in ethylene (EC) and propylene carbonate (PC) (1:1 in volume, 5% FEC) as the electrolyte. The charge-discharge measurements were tested using a Land battery testing station. CV tests were performed using a CHI electrochemical workstation at a scan rate of 0.1 mV s^{-1}. The batteries were charged for half an hour and relaxed under open circuit for 10 h at 0.1C for the GITT measurements.

2.4. DFT calculation

The spin-polarized DFT + U calculations were conducted using Vienna *ab* initio simulation package (VASP) [22]. The ion-electron interaction is described with the projector augmented wave (PAW) [23] pseudo-potentials with an energy cut-off of 520 eV while the exchange-correlation energy is described by the Perdew–Burke–Ernzerhof (PBE) [24] functional form of the generalized gradient approximation (GGA) [25]. The geometry optimiztion are performed using the conjugated gradient methode, and the convergence

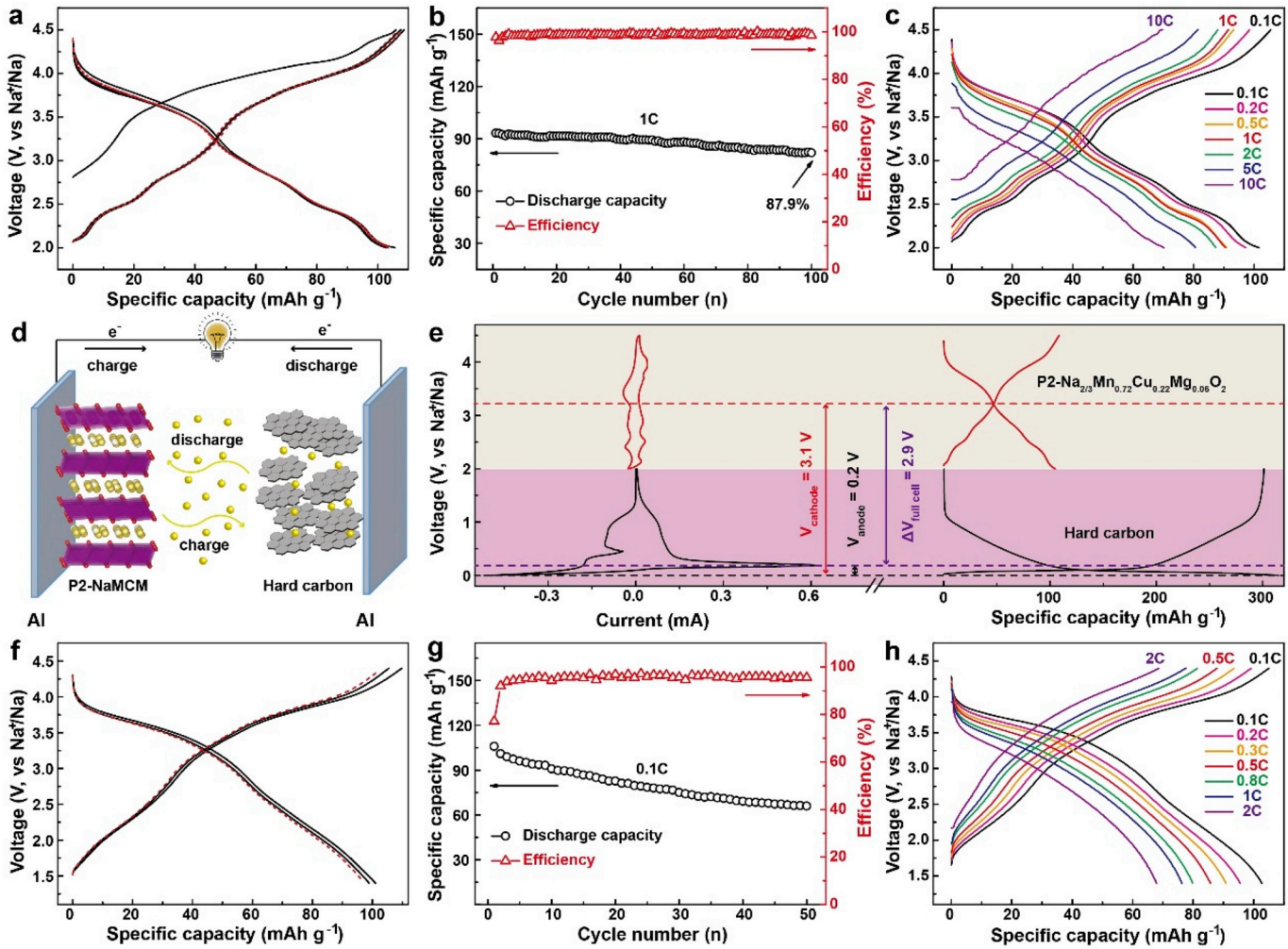

Fig. 2. (a) Galvanostatic charge/discharge voltage profiles of P2-NaMCM electrode in the voltage range of 2.0–4.5 V. (b) Corresponding cycling performance and (c) rate performance of P2-NaMCM electrodes. Electrochemical performance of full cell system coupling P2-NaMCM as cathode material and hard carbon as anode material. d) Schematic showing the discharge processes. e) Galvanostatic charge/discharge curves versus specific capacity of P2-NaMCM and hard carbon full cells. f) Cycling performance of P2-NaMCM and hard carbon full cells and (h) rate performance of full cells at various rates of in the voltage range of 1.4–4.5 V.

threshold is set to be 10^{-5} in energy and 0.01 eV/Å in force with the ***k***-grid of 4 × 4 × 2. To obtain the density of states, a larger ***k***-grid of 11 × 11 × 9 is used. The applied effective *U* correction of 4.0 eV was added to remove the spurious self-interaction of the Mn d-electrons as previous work [21].

3. Results and discussions

Since phase-pure sample cannot be obtained when copper content surpass 22% in P2-$Na_{2/3}Mn_{1-x}Cu_xO_2$, extra 6% Mg is incorporated to obtain pure phase P2-$Na_{2/3}Mn_{0.72}Cu_{0.22}Mg_{0.06}O_2$ [26]. The X-ray diffraction (XRD) pattern of the P2-$Na_{2/3}Mn_{0.72}Cu_{0.22}Mg_{0.06}O_2$ (hereafter denoted as P2-NaMCM) material in Fig. 1a can be well indexed to the hexagonal $P6_3/mmc$ space group without any impurity. The refined lattice parameters were $a = b = 2.8965$ (5) Å and $c = 11.191$ (0) Å and detailed crystallographic data are summarized in Table S1. The structure of the P2-NaMCM phase is illustrated in the inset of Fig. 1a, which is composed of alternate Na layers (3.559 Å) and MO_2 layers (2.036 Å) with close ABBA oxygen-ion framework packing along the *c*-axis direction (Fig. S1). The refined occupancies of edge-sharing Na_e (2d Wyckoff sites) and face-sharing Na_f (2b Wyckoff sites) are 0.401 and 0.269, respectively. This P2-NaMCM compound is consisted of the plate-like particles with the size distribution of 10–20 μm (Fig. 1b). The neighboring distance of (002) crystallographic planes is measured to be 5.6 Å by the high-resolution transmission electron microscopy (HRTEM) image (Fig. 1c). The P2 phase was further analyzed by annular bright field (ABF) and high-angle annular dark field (HAADF)-scanning transmission electron microscopy (STEM) with atomic resolution (Fig. S2). The enlarged HAADF-STEM image (Fig. 1d) at [010] zone axis demonstrate that the interslab distance (d_c) is 5.59 Å, matching well with the refined XRD data. From the enlarged ABF-STEM observations of octahedral MO_2 at the [010] zone axis, the Na and MO_2 layers stack alternately with a distinct ABBA-stacking mode for the O columns. And every two layers of MO_2 show a typical P2 phase mirroring symmetry as inserted in Fig. 1e for convenient visualization [27,28]. The selected area electron diffraction (SAED) in Fig. S3 at [001] direction further confirms that typical hexagonal symmetric arrangement of the transition metal atoms. Energy dispersive spectroscopy (EDS) elementary mapping suggests an even distribution of the sodium, manganese, copper, magnesium and oxygen elements in the sample (Fig. 1f).

The electrochemical properties of P2-NaMCM was tested in Na/P2-NaMCM half cells between 2.0 and 4.5 V at a 0.1C rate (1C = 174 mA g^{-1}). The charge capacity of 108.0 mA h g^{-1} in Fig. 2a, corresponding to 0.42 sodium removal, is much higher than the capacity from removal of 0.15 Na solely through the oxidation of Mn^{3+} to Mn^{4+} (assuming the average Mn oxidation state is +3.85 derived from Fig. S4). Therefore, Cu or O might participates in charge compensation to contribute the extra capacity. Upon subsequent discharging to 2.0 V,

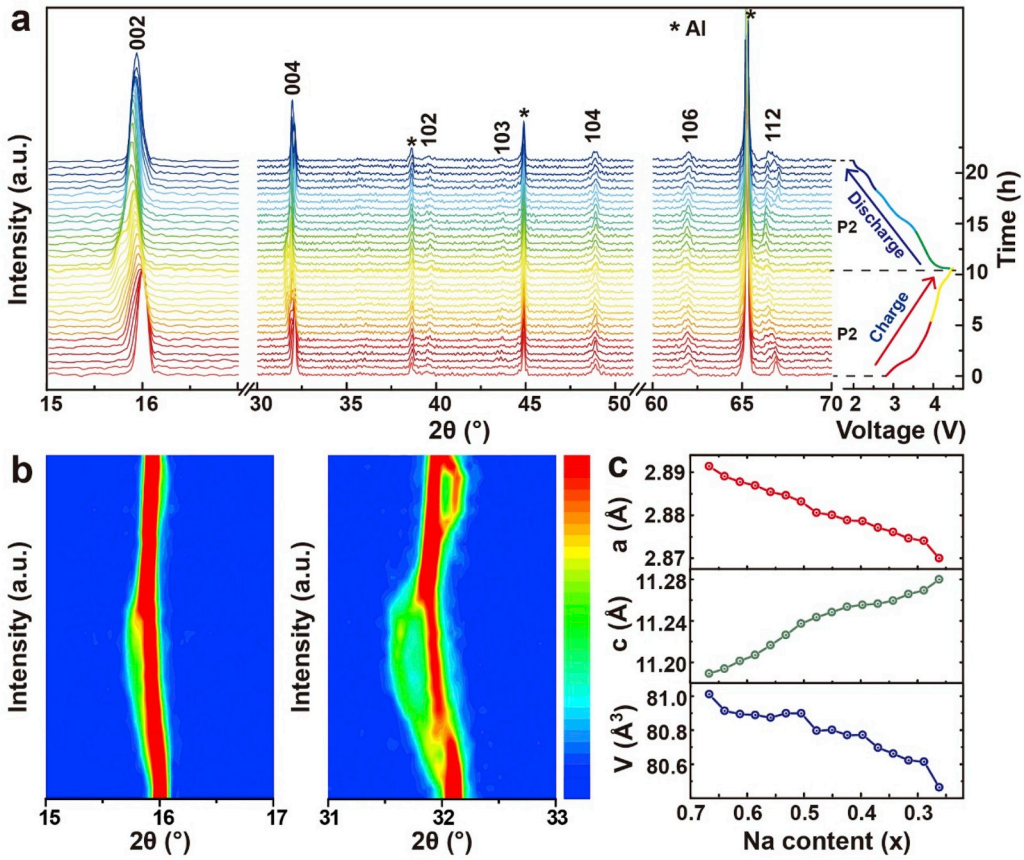

Fig. 3. (a) *In-situ* XRD patterns collected during the first charge/discharge of the Na/NaMCM cell under a current rate of 0.1C at voltage range between 2.0 and 4.5 V. Black asterisks represent peaks from Al window. (b) The corresponding contour map of (002) and (004) peaks of operando XRD patterns. (c) Lattice parameters evolution of Na_xMCM as a function of Na^+ content.

the material uptake the almost identical sodium (0.42) with a high initial Coulombic efficiency of 99.6% and a reversible capacity of 107.6 mA h g^{-1} (Fig. 2a). The cause of obvious voltage hysteresis between the initial charge and discharge curve is likely to be caused by partial O loss during oxygen oxidization and reduction [17]. Cyclic voltammograms (CV) charaterization at a scan rate of 0.1 mV s^{-1} (Fig. S5) manifest four pairs of redox peaks. The three peaks at 2.12/2.01, 2.51/2.40, 2.88/2.80 refer to Mn^{3+}/Mn^{4+} for three Na-vacancy ordering induced peaks between 2.0 and 3.0 V and the peak at 3.97/3.41 is attributed to Cu^{2+}/Cu^{3+}. An extra peak located at 4.23 V might imply possible oxygen oxidization during overcharge process. The insertion of extra sodium in P2-$Na_{2/3}Mn_{0.72}Cu_{0.22}Mg_{0.06}O_2$ is highly reversible, leading to a stable specific capacity of ≈93 mA h g^{-1} at 1C rate and maintain almost 87.9% of initial capacity after 100 cycles (Fig. 2b). In addition, the structure and morphology integrity of P2-NaMCM material are also well maintained after 100 cycles (Fig. S6). P2-$Na_{2/3}Mn_{0.72}Cu_{0.22}Mg_{0.06}O_2$ cathodes also show very small polarization (Fig. S7), ensuring a high rate capability with 107.6, 97.3, 91.0, 90.5, 87.4, 80.7 and 70.3 mA h g^{-1} at 0.1C, 0.2C, 0.5C, 1C, 2C, 5C and 10C, respectively (Fig. 2c). When P2-$Na_{2/3}Mn_{0.72}Cu_{0.22}Mg_{0.06}O_2$ was deeply discharged to 1.5 V, a large capacity of 158.8 mA h g^{-1} was achieved (Fig. S8). However, this material shows poor cycling stability with only 32.9% capacity retention after 50 cycles at 0.1C, which can be ascribed to more Jahn-Teller active Mn^{3+} ions incorporated into this structure after deep discharge [29,30].

By coupling with hard carbon anode, the electrochemical performance of P2-NaMCM cathodes were also evaluated in P2-NaMCM/C full cells (Fig. 2d). Before assembling the full batteries, the carbon anode was evaluated. The microstructure of and mophology of hard carbon was charaterized using XRD, Raman (Fig. S9) and SEM (Fig. S10), while the electrochemical properties of hard carbon anodes was evaluated in Na/C half cells with metallic sodium foil as counter electrode (Fig. S11). To determin the full cell charge/discharge voltage window and mass ratio of P2-NaMCM cathode to carbon anode, CV and galvanostatic charging/discharging profiles of P2-NaMCM and hard carbon in half cells were intergrated in Fig. 2e. The electrochemical properties of P2-NaMCM/hard carbon full cells were ultimately tested at 0.1C in the voltage range of 1.4–4.5 V. The P2-NaMCM/hard carbon full cell with P/N capacity ratio of 1.3 exhibits a discharge capacity of 106.9 mAh·g^{-1} in the first cycle (Fig. S12). The initial Coulombic efficiency of 75.3% can be attributed to the formation of a solid electrolyte interphase (SEI) on the hard carbon anode [31]. As displayed in Fig. 2f, the reversible capacity is around 101.0 mA h g^{-1} during the sequent cycles, and the capacity retention approaches 62.2% on the next 50 cycles (Fig. 2g). The P2-NaMCM/hard carbon full cell also shows superior rate performance, as demonstrated in Fig. 2h, P2-NaMCM can still deliver 66.8 mA h g^{-1} even at a relatively high rate of 2C (348 mA g^{-1}).

The structure evolution of P2-NaMCM cathodes during Na^+ extraction/insertion were investigated using operando XRD in the Na/P2-NaMCM half-cells (Fig. 3a). Upon Na extraction (charge), the P2 (002) and (004) diffraction lines move toward a lower angle due to the enlarged electrostatic repulsion between neighboring MO_2 slabs, while (100), (102), and (103) peaks consecutively shift to a higher angle with the contracted *ab* plane. After further extraction of 0.42 Na to the end of charge, no extra peaks beyond the P2 phase are detected, suggesting the extraction of the 0.42 Na at a high potential accompany with a solid solution reaction mechanism [32]. Noting that the rearrangement of the different in-plane Na^+-vacancy orderings make the shape of the (004) peak become asymmetric broadening during Na removal (Fig. 3b) [33, 34]. Upon the subsequent discharge to 2.0 V, the characteristic peak of the charged phase (00l peak) recovers and moves toward higher angles

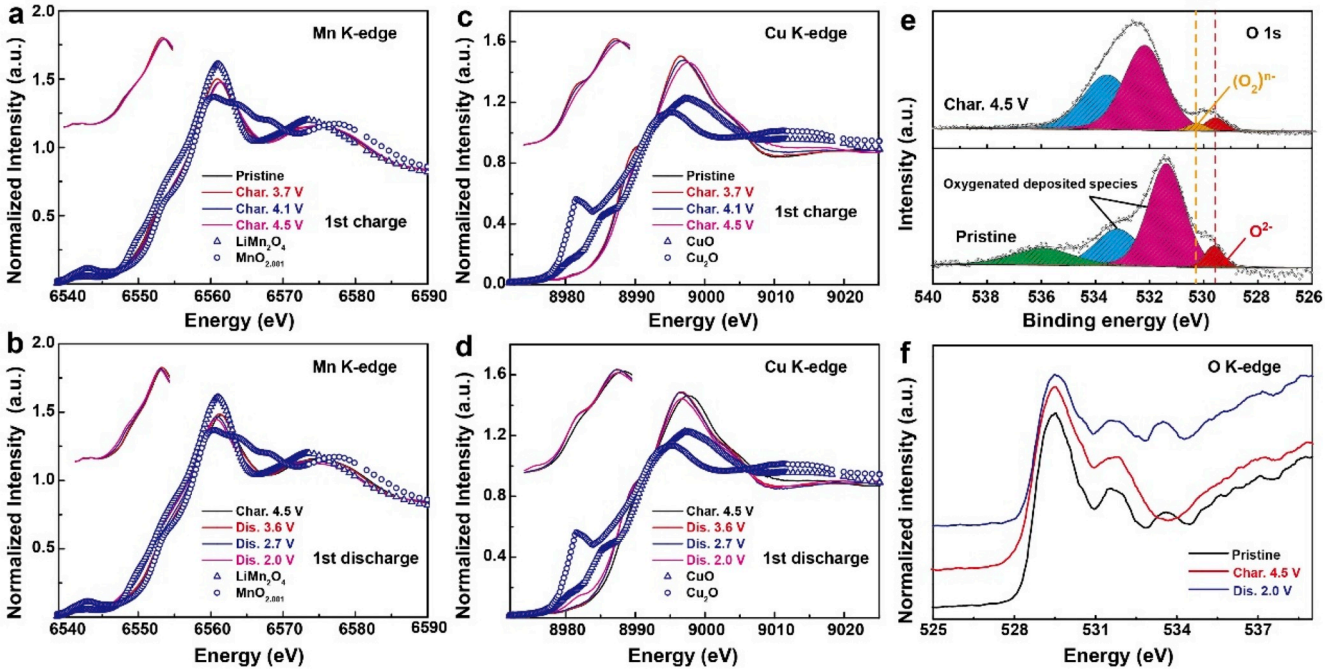

Fig. 4. *Ex situ* XANES spectra at the (a, b) Mn K-edge and (c, d) Cu K-edge of Na_xMCM electrodes collected at different charge/discharge states. (e) *Ex situ* XPS O 1s spectra of Na_xMCM samples upon the first charge. (f) sXAS O K-edge spectra collected at different states in PFY mode.

manifesting a sequential decrease of the interlayer distance until (002) Bragg peak reach the diffraction angle of the P2-type structure for the composition x = 0.67. Accompanied by more Jahn-Teller active MnIII (t_{2g}^3-e_g^1) incorporated into this structure, P′2 phase formed when further deep discharged to 1.5 V, incurring an obvious voltage plateau around 1.9 V (Fig. S8b) [35,36]. Lattice parameters evolution of Na_xMCM as a function of Na content is shown in Fig. 3c. The *a* lattice parameter is contracting due to reduced ionic radius of Cu^{2+} and Mn^{3+} during oxidization upon Na^+ extraction. The *c* axis is expanding due to an increase in electrostatic repulsion between adjacent oxygen layers [37]. At the fully charged state, the intensity of the (002) diffraction line appeared at 15.9° and the unit cell volume variation of P2-NaMCM before and after Na removal is only −0.68%, matching well with the stable cycling performance at 0.1C.

In addition to structure change, the charge compensation of Na_xMCM upon Na ions extraction/insertion was also investigated using hard X-ray absorption spectroscopy at Mn and Cu K-edges. As displayed in Fig. 4a, the original Mn oxidation state is slightly lower than tetravalent. The X-ray absorption near-edge structure (XANES) spectrum at Mn K-edge shows a shift toward high-energy edge position, which is consistent with the complete oxidation to +4. Besides, the suppressed shoulder feature located at 6551 eV suggests that the Mn electronic density of states is redistributed [21]. Upon Na intercalation, the Mn XANES spectra maintains the shape and edge position until the sample discharge to 2.7 V. Then the Mn is reduced after fully discharged to 2 V, which is evidenced by the restored shoulder feature and a shift toward lowest energy (Fig. 4b). The Cu K-edge XANES spectrum show a slight shift toward higher energy region after deep charge to 4.5 V and move back to pristine position upon Na insertion (Fig. 4c and d), indicating that divalent copper is oxidized to a higher Cu^{3+} valence state. The shoulder peak located at 8995 eV also shows an obvious variation, which implies that the Cu–O local environment is largely changed due to the mitigated Jahn-Teller effect of CuIII (t_{2g}^6-e_g^2) and MnIV (t_{2g}^3-e_g^0) during charge [38]. XANES results confirm the electrochemical reaction is mainly compensated by reversible Mn and Cu changes. Extended X-ray absorption fine structure (EXAFS) spectra (Fig. S13) indicate constant Mn–O and Cu–O distances around 1.50 Å. Shorter ones characteristic of larger oxidation state of Mn/Cu in the full charged sample are observed.

O (1s) XPS spectrum is an effective tool to identify the oxygen-related species, crystalline network of layered oxides commonly exhibits a characteristic O^{2-} anions peak at 529.5 eV (Fig. 4e) [39]. Additional peaks mainly originate from contamination at the surface of the sample by hydroxyl-like or oxygenated species [40]. Obviously, an additional component at 530.5 eV is need to introduce to fit the asymmetric shape of the O (1s) main peak correctly after full charge. This additional O (1s) component might be ascribed to the participation of the O^{2-} anion during the redox process, resulting in a decreased negative charge for an "oxidized" oxygen $(O_2)^{n-}$ [41]. O K-edge soft X-ray absorption spectroscopy (sXAS) spectra were collected using partial fluorescence yield (PFY) mode to further confirm the anionic redox (Fig. 4f). The edge peak near 530 eV originate from the transitions between transition metal 3d and O 2p orbitals, and the edge peak at 534 eV refers to vacancy O. The edge of the hybridized peaks show a slight shift to the lower energy region and the oxygen vacancy peak disappeared for the charged samples, which is ascribed to the induced electron filling and extraction within O 2p band by oxygen redox [42,43]. Therefore, above results demonstrate that Mn^{3+}/Mn^{4+}, Cu^{2+}/Cu^{3+} and $O^{2-}/(O_2)^{n-}$ redox couples are involved in the charge compensation during the electrochemical process in agreement with the observed 0.42 e^- transfer.

To further explore the nature of anionic redox activity observed in P2-NaMCM, we performed DFT calculations. On the basis of the projected density of states of P2-NaMCM, Cu 3d orbitals is largely overlapped with O (2p) states at the highest occupied states, suggesting O 2p orbital a exhibits significant orbital hybridization with the Cu 3d orbital at the Fermi level [16,44]. Thus redox couple involving losing (oxidizing) or adding (reducing) electrons in the Cu 3d and O 2p orbital become available. Compared with the Mg–O [20] or Zn–O [21] bonds reported by Bruce and Tarascon et al., Cu will have its non-flled d^9 band with the oxygen states so that Cu 3d orbitals can interact with the oxygen (O) because of its large electronegative character as compared with Mg, Zn. Therefore a larger covalence of the Cu–O bond is obtained with respect to Zn–O and Mg–O bond, leading to oxidation of the O (2p) states during charge and discharge [21,45]. The redox chemistry can be further reconciled by using the relationship of energy versus density of states (Fig. 5b and c). During the first charging from the open-circuit voltage to 3.0 V, Mn^{3+} (t_{2g}^3-e_g^1) oxidizes to Mn^{4+} (t_{2g}^3-e_g^0) by losing an

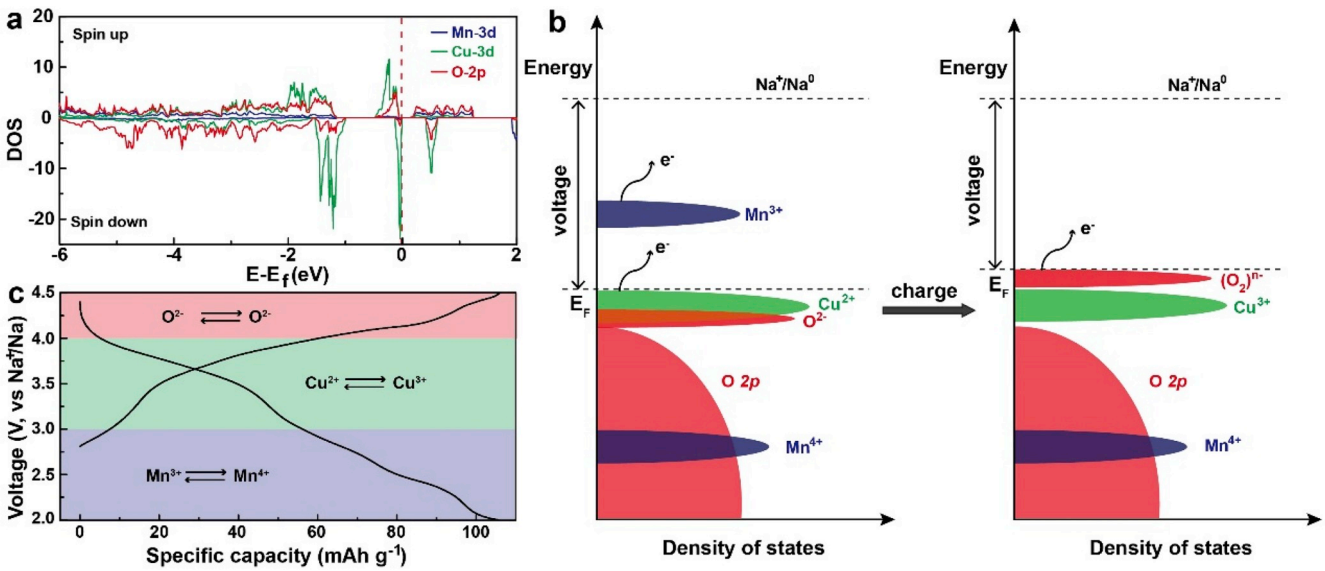

Fig. 5. (a) The calculated density of states (DOS) of P2-NaMCM. (b) Schematic that illustrates the energy versus density of states in the sodium-deficient phase of P2-NaMCM. (c) Charge compensation of different elements' contribution during the charge and discharge process.

electron in e_g orbital. Then Cu^{2+} (t_{2g}^6-e_g^3) began to participate in charge compensation on charging from 3.0 to 4.0 V. On further charging from 4.0 to 4.5 V, the electrons will lose in oxygen valence bond. Upon first discharge, partial oxygen ions are reduced from 4.5 V to 4.0 V; then Cu^{3+} ions and Mn^{4+} ions are reduced within the voltage range of 4.0–3.0 V and 3.0–2.0 V, respectively. In the subsequent charge/discharge process, the valence states of Mn, Cu, and O undergo reversible changes, thus promoting the following reversible electrochemical reaction.

4. Conclusions

In summary, we have studied a Na-deficient layered P2-$Na_{2/3}Mn_{0.72}Cu_{0.22}Mg_{0.06}O_2$ phase having a strong electronegative copper element within the transition metal slabs that shows both cationic and anionic redox activity. Mn^{3+}/Mn^{4+}, Cu^{2+}/Cu^{3+} and $O^{2-}/(O_2)^{n-}$ all contribute to the redox reaction upon Na^+ ions extraction and insertion by the combined analysis of hard and soft X-ray absorption spectra. The existence of strong covalency between Cu 3d and O 2p orbitals promises cationic and anionic redox chemistry in this material by DFT calculations. *In situ* XRD technique confirmed a solid solution reaction mechanism accompanied by some Na ordering rearrangement during battery cycling. As a result, the P2-$Na_{2/3}Mn_{0.72}Cu_{0.22}Mg_{0.06}O_2$ cathode exhibited a reversible discharge capacity of 107.6 mA h g^{-1} with good capacity retention (≈87.9% at 1C after 100 cycles) in Na half cells. This study provides us a solid platform to clearly decipher the relationship between redox chemistry and molecular orbital in layered Na cathode materials.

Declaration of competing interest

The authors declare no competing financial interest.

Acknowledgements

This work was supported by the US Department of Energy (DOE) (No. DEEE0008202). Q.C.W. and X.-Q.Y. were supported by the Assistant Secretary for Energy Efficiency and Renewable Energy, Vehicle Technology Office of the US Department of Energy through the Advanced Battery Materials Research Program, including Battery500 Consortium under contract DE-SC0012704. This research used beamlines 7-BM of the National Synchrotron Light Source II, a DOE Office of Science User Facility operated for the DOE Office of Science by Brookhaven National Laboratory under contract DE-SC0012704.

Appendix A. Supplementary data

Supplementary data to this article can be found online at https://doi.org/10.1016/j.nanoen.2020.104474.

References

[1] M. Armand, J.M. Tarascon, Nature 451 (2008) 652.
[2] N. Yabuuchi, K. Kubota, M. Dahbi, S. Komaba, Chem. Rev. 114 (2014) 11636.
[3] K.Z. Jiang, S. Xu, S.H. Guo, X.Y. Zhang, X.P. Zhang, Y. Qiao, T.C. Fang, P. Wang, P. He, H.S. Zhou, Nano Energy 52 (2018) 88.
[4] J.-Y. Hwang, S.-T. Myung, Y.-K. Sun, Chem. Soc. Rev. 46 (2017) 3529.
[5] P.-F. Wang, Y. You, Y.-X. Yin, Y.-G. Guo, Adv. Energy Mater. 8 (2018) 1701912.
[6] K. Kubota, S. Kumakura, Y. Yoda, K. Kuroki, S. Komaba, Adv. Energy Mater. 8 (2018) 1703415.
[7] Y.-N. Zhou, P.-F. Wang, Y.-B. Niu, Q. Li, X. Yu, Y.-X. Yin, S. Xu, Y.-G. Guo, Nano Energy 55 (2019) 143.
[8] J. Hong, W.E. Gent, P. Xiao, K. Lim, D.H. Seo, J. Wu, P.M. Csernica, C.J. Takacs, D. Nordlund, C.J. Sun, K.H. Stone, D. Passarello, W. Yang, D. Prendergast, G. Ceder, M.F. Toney, W.C. Chueh, Nat. Mater. 18 (2019) 256.
[9] Y. Zuo, B. Li, N. Jiang, W. Chu, H. Zhang, R. Zou, D. Xia, Adv. Mater. 30 (2018) 1707255.
[10] X. Li, Y. Qiao, S. Guo, K. Jiang, M. Ishida, H. Zhou, Adv. Mater. 31 (2019) 1807825.
[11] A.J. Perez, Q. Jacquet, D. Batuk, A. Iadecola, M. Saubanère, G. Rousse, D. Larcher, H. Vezin, M.-L. Doublet, J.-M. Tarascon, Nat. Energy 2 (2017) 954.
[12] A.J. Perez, D. Batuk, M. Saubanère, G. Rousse, D. Foix, E. McCalla, E.J. Berg, R. Dugas, K.H.W. van den Bos, M.-L. Doublet, D. Gonbeau, A.M. Abakumov, G. Van Tendeloo, J.-M. Tarascon, Chem. Mater. 28 (2016) 8278.
[13] C. Ma, J. Alvarado, J. Xu, R.J. Clement, M. Kodur, W. Tong, C.P. Grey, Y.S. Meng, J. Am. Chem. Soc. 139 (2017) 4835.
[14] P. Rozier, M. Sathiya, A.-R. Paulraj, D. Foix, T. Desaunay, P.-L. Taberna, P. Simon, J.-M. Tarascon, Electrochem. Commun. 53 (2015) 29.
[15] M. Otoyama, Q. Jacquet, A. Iadecola, M. Saubanere, G. Rousse, J.M. Tarascon, Adv. Energy Mater. 9 (2019) 1803674.
[16] M.H.N. Assadi, M. Okubo, A. Yamada, Y. Tateyama, J. Mater. Chem. A 6 (2018) 3747.
[17] R.A. House, U. Maitra, L. Jin, J.G. Lozano, J.W. Somerville, N.H. Rees, A.J. Naylor, L.C. Duda, F. Massel, A.V. Chadwick, S. Ramos, D.M. Pickup, D.E. McNally, X. Lu, T. Schmitt, M.R. Roberts, P.G. Bruce, Chem. Mater. 31 (2019) 3293.
[18] Y. Qiao, S.H. Guo, K. Zhu, P. Liu, X. Li, K.Z. Jiang, C.J. Sun, M.W. Chen, H.S. Zhou, Energy Environ. Sci. 11 (2018) 299.
[19] X. Rong, E. Hu, Y. Lu, F. Meng, C. Zhao, X. Wang, Q. Zhang, X. Yu, L. Gu, Y.-S. Hu, H. Li, X. Huang, X.-Q. Yang, C. Delmas, L. Chen, Joule 3 (2019) 503.
[20] U. Maitra, R.A. House, J.W. Somerville, N. Tapia-Ruiz, J.G. Lozano, N. Guerrini, R. Hao, K. Luo, L. Jin, M.A. Perez-Osorio, F. Massel, D.M. Pickup, S. Ramos, X. Lu, D.E. McNally, A.V. Chadwick, F. Giustino, T. Schmitt, L.C. Duda, M.R. Roberts, P. G. Bruce, Nat. Chem. 10 (2018) 288.

[21] X. Bai, M. Sathiya, B. Mendoza-Sánchez, A. Iadecola, J. Vergnet, R. Dedryvère, M. Saubanère, A.M. Abakumov, P. Rozier, J.-M. Tarascon, Adv. Energy Mater. 8 (2018) 1802379.
[22] P. Hohenberg, W. Kohn, Phys. Rev. 136 (1964) B864.
[23] P.E. Blöchl, Phys. Rev. B 50 (1994) 17953.
[24] J.P. Perdew, K. Burke, M. Ernzerhof, Phys. Rev. Lett. 77 (1996) 3865.
[25] G. Kresse, J. Furthmüller, Phys. Rev. B 54 (1996) 11169.
[26] W. Kang, Z. Zhang, P.-K. Lee, T.-W. Ng, W. Li, Y. Tang, W. Zhang, C.-S. Lee, D. Y. Wai Yu, J. Mater. Chem. A 3 (2015) 22846.
[27] S. Guo, P. Liu, H. Yu, Y. Zhu, M. Chen, M. Ishida, H. Zhou, Angew. Chem. Int. Ed. 54 (2015) 5894.
[28] X. Lu, Y. Wang, P. Liu, L. Gu, Y.S. Hu, H. Li, G.P. Demopoulos, L. Chen, Phys. Chem. Chem. Phys. 16 (2014) 21946.
[29] S. Kumakura, Y. Tahara, K. Kubota, K. Chihara, S. Komaba, Angew. Chem. Int. Ed. 55 (2016) 12760.
[30] J. Billaud, G. Singh, A.R. Armstrong, E. Gonzalo, V. Roddatis, M. Armand, T. Rojo, P.G. Bruce, Energy Environ. Sci. 7 (2014) 1387.
[31] Y. Li, Y.F. Yuan, Y. Bai, Y.C. Liu, Z.H. Wang, L.M. Li, F. Wu, K. Amine, C. Wu, J. Lu, Adv. Energy Mater. 8 (2018) 1702781.
[32] P.-F. Wang, H.-R. Yao, X.-Y. Liu, Y.-X. Yin, J.-N. Zhang, Y. Wen, X. Yu, L. Gu, Y.-G. Guo, Sci. Adv. 4 (2018) eaar6018.
[33] R. Berthelot, D. Carlier, C. Delmas, Nat. Mater. 10 (2011) 74.
[34] A. Gutierrez, W.M. Dose, O.J. Borkiewicz, F. Guo, M. Avdeev, S. Kim, T.T. Fister, Y. Ren, J. Bareño, C.S. Johnson, J. Phys. Chem. C 122 (2018) 23251.
[35] Q.C. Wang, J.K. Meng, X.Y. Yue, Q.Q. Qiu, Y. Song, X.J. Wu, Z.W. Fu, Y.Y. Xia, Z. Shadike, J. Wu, X.Q. Yang, Y.N. Zhou, J. Am. Chem. Soc. 141 (2019) 840.
[36] S. Kumakura, Y. Tahara, S. Sato, K. Kubota, S. Komaba, Chem. Mater. 29 (2017) 8958.
[37] J.W. Somerville, A. Sobkowiak, N. Tapia-Ruiz, J. Billaud, J.G. Lozano, R.A. House, L.C. Gallington, T. Ericsson, L. Häggström, M.R. Roberts, U. Maitra, P.G. Bruce, Energy Environ. Sci. 12 (2019) 2223.
[38] L. Mu, S. Xu, Y. Li, Y.-S. Hu, H. Li, L. Chen, X. Huang, Adv. Mater. 27 (2015) 6928.
[39] E. Zhao, Q. Li, F. Meng, J. Liu, J. Wang, L. He, Z. Jiang, Q. Zhang, X. Yu, L. Gu, W. Yang, H. Li, F. Wang, X. Huang, Angew. Chem. Int. Ed. 58 (2019) 4323.
[40] C. Zhao, Q. Wang, Y. Lu, L. Jiang, L. Liu, X. Yu, L. Chen, B. Li, Y.-S. Hu, Energy Storage Mater. 20 (2019) 395.
[41] X. Zhang, Y. Qiao, S. Guo, K. Jiang, S. Xu, H. Xu, P. Wang, P. He, H. Zhou, Adv. Mater. 31 (2019) 1807770.
[42] P.E. Pearce, A.J. Perez, G. Rousse, M. Saubanere, D. Batuk, D. Foix, E. McCalla, A. M. Abakumov, G. Van Tendeloo, M.L. Doublet, J.M. Tarascon, Nat. Mater. 16 (2017) 580.
[43] X. Rong, J. Liu, E. Hu, Y. Liu, Y. Wang, J. Wu, X. Yu, K. Page, Y.-S. Hu, W. Yang, H. Li, X.-Q. Yang, L. Chen, X. Huang, Joule 2 (2018) 125.
[44] B.H. Song, M.X. Tang, E.Y. Hu, O.J. Borkiewicz, K.M. Wiaderek, Y.M. Zhang, N. D. Phillip, X.M. Liu, Z. Shadike, C. Li, L.K. Song, Y.Y. Hu, M.F. Chi, G.M. Veith, X. Q. Yang, J. Liu, J. Nanda, K. Page, A. Huq, Chem. Mater. 31 (2019) 3756.
[45] Y. Nanba, T. Iwao, B.M.d. Boisse, W. Zhao, E. Hosono, D. Asakura, H. Niwa, H. Kiuchi, J. Miyawaki, Y. Harada, M. Okubo, A. Yamada, Chem. Mater. 28 (2016) 1058.

Dr. Peng-Fei Wang received his P h.D. degree in Phisical Chemistry from Institute of Chemistry, Chinese Academy of Sciences (2018). He is currently a postdoctoral fellow at University of Maryland-College Park. His research focus on high performance cathodes for lithium/sodium-ion batteries.

Dr. Yao Xiao received his Ph.D. degree from Sichuan University in 2019. He was a visiting scholar at Institute of Chemistry, Chinese Academy of Sciences (ICCAS) from 2016 to 2019. He is currently a postdoctoral fellow at the School of Materials Science and Engineering, Nanyang Technological University, Singapore. His research focuses on nanostructured electrode materials for advanced lithium-ion and sodium-ion batteries.

Nan Piao is a Ph.D. candidate at Institute of Nuclear and New Energy Technology, Tsinghua University. She is a visiting scholar at University of Maryland-College Park. Her researches focus on lithium-ion batteries and lithium-metal batteries.

Qin-Chao Wang is currently working as postdoctoral researcher at Fudan University and is a visiting scholar at Brookhaven National Laboratory. He received his Ph.D. degree in Materials Physics and Chemistry from Fudan University in 2018. His research interests focus on design and synthesis novel cathode materials and studying their high performance for sodium-ion batteries and energy application.

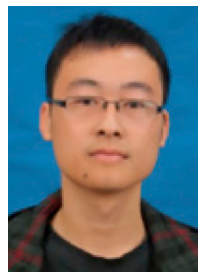

Dr. Xiao Ji received his Ph.D. degree in Electronic Science and Technology, Huazhong University of Science and Technology. He is currently a postdoctoral fellow at Department of Chemical and Biomolecular Engineering, University of Maryland-College Park. His research interest is mainly focused on First-principles calculations Li-ion batteries and supercapacitor.

Ting Jin received her B.S. degree in materials chemistry from Northwest University (China) in 2015. Currently, she is a PhD student in the group of Prof. Lifang Jiao at Nankai University (China). Her research interests focus on design and fabrication of advanced electrode materials for energy storage and conversion, such as rechargeable lithium-ion and sodium-ion batteries.

Yu-Jie Guo received her bachelor's degree from Qingdao University in 2017. She is currently a Ph. D candidate under the supervision of Prof. Yu-Guo Guo at the Institute of Chemistry, Chinese Academy of Sciences. Her research focuses on advanced electrode materials for rechargeable sodium-ion batteries.

Sufu Liu started his Ph.D. degree in Department of Materials Science and Engineering, Zhejiang University. He is currently a joint Ph.D. candidate at Department of Chemical and Biomolecular Engineering, University of Maryland-College Park. His research interest is mainly focused on the all-solid-state batteries and the modification of Li metal anode.

Tao Deng is currently a PhD candidate in the Department of Chemical and Biomolecular Engineering at University of Maryland-College Park. He received his bachelor's degree from Tianjin University (2014) and M.Sc. degree from Rice University (2016). His research interests focus on electrochemistry and interface chemistry for high-energy Li/Na metal batteries.

Chunyu Cui received his bachelor degree, and is currently a Ph. D. candidate, at College of Chemistry and Chemical Engineering, Hunan University. His research interests are design of materials structure to achieve the high performance of LIBs and NIBs.

Dr. Long Chen received his Ph.D. degree in Phisical Chemistry from Fudan University. He is currently an assistant research scientist at University of Maryland-College Park. His research focus on Lithium ion batteries and other novel electrochemical energy storage systems.

Yu-Guo Guo is a Professor of Chemistry at ICCAS. He received his Ph.D. in Physical Chemistry from ICCAS in 2004. He worked at the Max Planck Institute for Solid State Research at Stuttgart (Germany) first as a Guest Scientist and then a Staff Scientist from 2004 to 2007. He joined ICCAS as a full professor in 2007. His research focuses on nanostructured energy materials and electrochemical energy storage devices, such as Li-ion, Li–S, solid lithium batteries and sodium-ion batteries.

Dr. Xiao-Qing Yang is the group leader of the electrochemical energy storage group in the Chemistry Division of Brookhaven National Laboratory (BNL). He is the Principal Investigator (PI) for several Battery Material Research (BMR) programs at BNL including Battery 500 Consortium funded by the Vehicle Technology Office, EE&RE, U.S. Department of Energy (USDOE). He received his B.S. in Material Science from Shannxi Mechanic Engineering Institute in Xi'an, China in 1976 and Ph. D. in Physics, from University of Florida, Gainesville, Florida USA in 1986. He received the "2012 Vehicle Technologies Program R&D Award" from the Vehicle Technologies Office of EE&RE, USDOE in May, 2012. In January 2015, he received the IBA2015 Research award from the International Battery Association (IBA). He was named to 2018 Highly Cited Researchers List, which recognizes influential researchers whose work ranks in the top one percent of the world's most-cited scientific papers.

Prof. Chunsheng Wang is a full professor at University of Maryland College Park. He was educated in materials science and trained in electrochemistry and got his Ph.D. degree from Zhejiang University. He has more than 150 peer-reviewed journal publications and more than 25 years of experience in battery research. His Li ion battery research has been highlighted in EFRC news by DoE in 2012, and by Chemical & Engineering News in 2013. He is a recipient of the University of Maryland Outstanding Junior Researcher Award.